CLEARANCE OF THE VAAC HARRIER CL002 FLIGHT CONTROL LAW USING μ-ANALYSIS TECHNIQUES

D.G. Bates*, R. Kureemun*, T. Mannchen†

* Department of Engineering, University of Leicester, University Road, Leicester LE1 7RH, UK, dgb3@le.ac.uk
† Institute of Flight Mechanics and Control, University of Stuttgart, Pfaffenwaldring 7a, 70550 Stuttgart, Germany

Keywords: Robustness Analysis, Flight Control, Aircraft

Abstract

We describe some new tools for the clearance of flight control laws for highly augmented aircraft. The tools are developed from general μ-analysis methods, and are applied to the clearance of a flight control law for a vertical/short take-off and landing aircraft. Stability robustness analysis results for the flight control law are presented in terms of the standard clearance criteria currently used by the European aerospace industry. Comparisons of the results obtained using μ-analysis and current approaches reveal that the new μ-tools provide more rigorous and efficient analysis of worst-case aircraft stability characteristics in the presence of multiple sources of parametric uncertainty.

1 Introduction

Modern high performance aircraft are often designed to be naturally unstable due to performance reasons and, therefore, can only be flown by means of a controller which provides artificial stability. As the safety of the aircraft is dependent on the controller, it must be proven to the clearance authorities that the controller functions correctly throughout the specified flight envelope in all normal and various failure conditions, and in the presence of all possible parameter variations. This task is a very lengthy and expensive process, particularly for high performance aircraft, where many different combinations of flight parameters (e.g. large variations in mass, inertia, centre of gravity positions, highly non-linear aerodynamics, aerodynamic tolerances, air data system tolerances, structural modes, failure cases, etc.) must be investigated so that guarantees about worst-case stability and performance can be made.

The aircraft models used for clearance purposes describe the actual aircraft dynamics, but only within given uncertainty bounds. One reason for this is the limited accuracy of the aerodynamic data set determined from theoretical calculations and wind tunnel tests. These parameters can even differ between two aircraft of the same type, due to production tolerances. Moreover, the employed sensor, actuator and hydraulic models are usually only approximations, where the nonlinear effects are not fully modelled because they are either not known or it would make the model unacceptably complex. The goal of the clearance process is to demonstrate that a set of selected criteria expressing stability and handling requirements is fulfilled. Typically, criteria covering both linear and non-linear stability, as well as various handling and performance requirements are used for the purpose of clearance. The clearance criteria can be grouped into four classes: linear stability criteria, aircraft handling/pilot induced oscillation (PIO) criteria, non-linear stability criteria and non-linear handling criteria. This paper focusses on the use of new analysis techniques for two linear stability criteria - details of the other clearance criteria can be found in [1].

To perform the clearance, for each point of the flight envelope, for all possible configurations and for all combinations of parameter variations and uncertainties, violations of the clearance criteria and the worst-case result for each criterion must be found. Based on the clearance results, flight restrictions are imposed where necessary. Faced with limited time and resources, the current flight clearance process employed by the European aerospace industry uses a gridding approach, [1], whereby the various clearance criteria are evaluated for all combinations of the extreme points of the aircraft's uncertain parameters. This process is then repeated over a gridding of the aircraft's flight envelope. Clearly, the effort involved in the resulting clearance assessment increases exponentially with the number of uncertain parameters. Another difficulty is the fact that there is no guarantee that the worst case uncertainty combination has in fact been found, since (a) it is possible that the worst-case combination of uncertain parameters does not lie on their extreme points, and (b) only a few selected points in the aircraft's flight envelope can be checked. This paper outlines briefly a new approach to the clearance problem based on the use of the structured singular value analysis method. For full details of the work described here the reader is referred to [2, 3].

2 Linear Stability Clearance Criteria

A basic requirement of the flight clearance process is to prove that the aircraft is stable over the entire flight envelope with sufficient margin against instability for all known uncertainties (worst-case combinations). The process consists of calculating linear stability margins for the open-loop frequency response in pitch, roll and yaw. These frequency responses are obtained by breaking the loop at the input of each actuator or of each sensor and are then plotted in Nichols diagrams where the required phase and gain margins are shown as exclusion regions which must not be violated by the plot.

In single loop analysis, the open-loop frequency response is obtained by breaking the loop at the input of each actuator or

sensor, one at a time, while leaving the other loops closed. For the nominal case, these Nichols plots should not violate the outer exclusion region shown in Figure 1, which corresponds to a minimum gain margin of ± 6 dB and a minimum phase margin of $\pm 35^o$. When uncertainties are taken into account, a boundary corresponding to ± 4.5 dB is used, as shown by the inner exclusion region in the same figure.

In multi loop analysis, the closed-loop system is required to withstand the application of simultaneous gain and phase offsets, defined by the regions shown in Figure 2, at the actuators or sensors without becoming unstable. To test for violations of this criterion, a perturbation of the form $K\left(\frac{1-Ts}{1+Ts}\right)$ is inserted at, for example, the input of each actuator. With K set to 1, T is then varied simultaneously in each loop until the eigenvalues of the closed-loop system go unstable. The phase margin is calculated as $\phi_{PM} = 2 * tan^{-1}\omega T$ where ω is the frequency of the generated undamped oscillation. K is then increased and decreased by 1.5 dB (corresponding to the right corner points of the Nichols exclusion region shown in Figure 2) and T is again varied for the new fixed gain until the eigenvalues become unstable. By setting T = 0 and varying K, the upper and lower gain margins can be obtained (corresponding to the left corner points of the Nichols diagram). These steps can be repeated for any number of points around the required Nichols exclusion region. Due to the fact that the criterion must be evaluated over all combinations of the aircraft's uncertain parameters, this test is in practice usually restricted to only a few points of the exclusion regions (e.g. the four corners of each exclusion region). In addition, the same gain and phase offsets are usually applied simultaneously in all loops, to avoid testing over too large a number of different combinations. Hence, it can be argued that this method can in practice lead to optimistic results.

In addition to the stability margin criterion, the eigenvalues of the closed-loop system must be calculated in order to identify possible unstable (i.e. those with positive real part) eigenvalues which do not appear in the Nichols plots. It is required to identify the flight cases where unstable eigenvalues occur and for what tolerance combination these eigenvalues have the largest real part. This test aims to determine the most severe cases of divergent modes in the closed-loop system in order to allow an assessment of their acceptability in terms of their influence on aircraft handling. A typical boundary on the real part of the eigenvalues is shown in Figure 3.

3 The HWEM Aircraft Model and Control Law

The Harrier Wide-Envelope Model (HWEM) is a full non-linear model of the Vectored-thrust Aircraft Advanced flight Control (VAAC) Harrier, developed by QinetiQ Ltd. for research on various aspects of flight control that are relevant to Short Take-Off and Vertical Landing (STOVL) operations. For the purposes of this study, the HWEM, originally implemented as a FORTRAN program, has been converted to a pure SIMULINK model. Data for the model was derived from a variety of sources, such as wind tunnel and flight test measurements and theoretical predictions, obtained from various aircraft [4]. The flight control surfaces comprise an all-moving tailplane, ailerons, flaps, rudder and airbrake. With the exception of the rudder, all control surfaces are hydraulically powered. The power-plant is a Rolls-Royce Pegasus Mk. 103 turbofan with four separate but coupled nozzles that allow the direction of the thrust to be altered. High-pressure bleed air from the engine compressor provides control at low speeds and hover, when the aerodynamic control surfaces become ineffective. The bleed air is ejected through reaction control valves (RCVs) in the wing tips (roll control), nose (pitch control) and tail boom (pitch and yaw control). Since the RCVs are mechanically linked to the appropriate control surfaces, the need for additional controls/actuators is avoided. Bleed air to the RCV's becomes progressively available as the nozzle angle is increased, the system being fully pressurised when nozzle angle exceeds 34^o.

The flight control law for the HWEM analysed in this study is based on VAAC Control Law 002 (CL002). It is a full three-axis (pitch, roll and yaw) control law designed using classical methods. The study reported in this paper considers the pitch axis only - for more details of this control law and of the lateral/directional control laws the reader is referred to [4].

Points in the flight envelope of the HWEM from 200 knots to hover are to be analysed in the clearance task, [3], and all flight conditions are defined for $1g$ straight and level flight at an altitude of 200 ft AMSL. The angle of attack range for all flight conditions is $[-4^o, +16^o]$. Five Category 1 (most significant) uncertain parameters are specified for the longitudinal axis analysis and are shown in Table 1. Further information about the uncertain aircraft parameters can be found in [4].

4 LFT-based Uncertainty Modelling

In order to apply μ-analysis tools to the HWEM model, the uncertainties in the original non-linear aircraft model must be represented in the form of linear fractional transformations (LFT's). In fact, it can be argued that the major difficulty in applying μ-analysis methods to real-world applications lies in this initial modelling step. In recent years, the subject of LFT-based uncertainty modelling has received much attention and has been found to be a very deep problem - see [5] for an overview. For linear systems, LFT-based uncertainty models can be derived numerically or physically from a given set of linearised equations of motions. The method necessitates the uncertain aircraft parameters to be explicitly defined in the equations of motion and is generally easy to implement. For non-linear systems, the problem of generating accurate LFT-based uncertainty models is much more difficult. In general, three different approaches can be identified, based on numerical methods, [6, 3], symbolic linearisation methods, [7, 3], and physical modelling methods, [5, 3].

The approach applied in this paper is that based on physical modelling principles. In this approach, the uncertainties are directly introduced in the non-linear SIMULINK model of the

aircraft in the form of multiplicative uncertainties, thus adding extra 'fictitious' inputs and outputs, w_i and z_i respectively, at the point in the system where the uncertainty Δ_1 occurs. This step is then repeated for each Δ_i representing the uncertainty in the other uncertain parameters. Now using standard block diagram manipulation software (e.g. the function **linmod** in MATLAB), the resulting non-linear model can be linearised to calculate the transfer matrix of the system M with inputs u = [w_1, ..., w_n, u_c] and outputs y = [z_1, ..., z_n, y_m], where u_c are the control inputs and y_m are the measured outputs. The LFT-based uncertainty model for the system is then given by the relation

$$y_m = F_u(M(s), \Delta)u_c \tag{1}$$

where Δ = *diag*(Δ_1, ..., Δ_n)

Clearly, the approach outlined above is simple and intuitive and allows an exact description of joint parametric dependencies in the model. Thus, it can be used to non-conservatively model the effect of the parametric uncertainties on the closed-loop system. As a result, the exact worst case set of uncertain parameters can be computed. If each uncertainty is introduced in only one location in the SIMULINK block diagram, the resulting LFT-based uncertainty model will also be of minimal order. In addition, this physical modelling approach allows additional uncertainties in the physical parameters (such as products of the uncertainties) to be easily implemented in the model.

The main limitation of the approach is that detailed information about the model and the uncertainties is required. Hence, its application is restricted to those models that can be implemented in a SIMULINK block diagram representation. Another drawback is that the dependence of the linearisations on the uncertain parameters is ignored, and therefore it is not clear how an LFT-based uncertainty model could be generated to capture variations in flight parameters such as the angle of attack or Mach number. Thus, unlike with numerical modelling approaches, it is not possible to easily generate LFT-based uncertainty descriptions that are valid over particular regions of the flight envelope.

To determine the accuracy of the derived LFT-based uncertainty model, it is vital, prior to any analysis, to validate it against the original linearised and nonlinear model. Full details of this process are given in [3]. Here, we give example results for an LFT-based uncertainty model of the HWEM generated at FC2. The five Category 1 longitudinal uncertainties from Table 1 are considered, and responses for inputs on tailplane, nozzle angle and throttle were generated, [3]. Sample results for a 1 deg step input to the tailplane are shown in Figure 4. Figure 5 shows the same case when a random combination of the uncertainties was used. In general, for small inputs, a good match was obtained between the non-linear and LFT-based models, although the match is not as good for random values of the uncertainties (Figure 5) as it is for the nominal case (Figure 4). This is to be expected, since the LFT-based model always uses the same linearisation, which would, of course, be changed by the variations in the uncertain parameters of the non-linear model.

5 μ-tools for evaluating clearance criteria

One approach for checking avoidance of Nichols exclusion regions using μ was proposed in [8, 9]. In this approach, the original Nichols exclusion regions shown in Figure 1 are replaced with elliptical regions centered around the critical point (-180,0) and satisfying the equation

$$\frac{|\ L(j\omega)\ |^2_{dB}}{G_m^{\ 2}} + \frac{(\angle L(j\omega)\ +\ 180)^2}{P_m^{\ 2}} = 1 \tag{2}$$

where $L(j\omega)$ is the open-loop frequency response, G_m is the desired gain margin and P_m is the desired phase margin.

Note that for elliptical regions corresponding to gain and phase margins of $\pm 6dB/\ \pm\ 36.87^\circ$ and $\pm 4.5dB/\ \pm\ 28.44^\circ$, respectively, the corresponding exclusion regions in the Nyquist plane are *circles* with (centre,radius) given by (-1.25,0.75) and (-1.14,0.54), [8, 3]. Now, as shown in [8], another way to interpret the requirement for avoidance of, for example, the circle (-1.14,0.54) in the Nyquist plane by the open-loop frequency response $L(j\omega)$, is to consider a plant subject to disc uncertainty of (centre,radius) given by (+1.14,0.54) at each frequency. It is then easy to see that avoidance of the (-1,0) critical point in the Nyquist plane by $L(j\omega)$ for all possible plants in this set is exactly equivalent to avoidance of the exclusion region B by $L(j\omega)$ for the original plant. The set of possible plants can be represented as

$$P(s) = P_1(s)(1.14 + \Delta_N) \tag{3}$$

where P_1 is the original plant, Δ_N is complex and $\|\ \Delta_N\ \|_\infty \leq 0.54$. This is of course the same as writing

$$P(s) = 1.14P_1(s)(1 + W_N\Delta_N) \tag{4}$$

with $W_N = 0.47$ and $\|\ \Delta_N\ \|_\infty \leq 1$. In this way we can represent the Nichols exclusion region as a 'fictitious' multiplicative input uncertainty for the scaled nominal plant. This uncertainty can then be pulled out of the closed loop system along with all the other uncertainties to form an LFT-based representation of the uncertain system in the usual way - see [10] for a simple example. For single-loop analysis, the 'fictitious' uncertainty representing the Nichols exclusion region is inserted in one loop at a time, while in the multi-loop case it is applied to all loops simultaneously. Note that this approach allows simultaneous variations of the uncertainty in all the loops of the system and thus every possible combination of the phase/gain offset is considered. In contrast, the classical approach assumes the same phase and gain margin variation in each loop and also checks for only a few points (usually the corners) in the exclusion region.

A second approach to casting Nichols plane exclusion region specifications as a μ problem was developed in [11]. This method models the Nichols exclusion regions of Figure 1 using a Padé approximation. The variations in the phase and gain are represented by equations (5) and (6) respectively. The phase

offset is given by

$$\phi = \left(\frac{\phi_{max} - \phi_{min}}{2}\right)\delta_2 + \left(\frac{\phi_{max} + \phi_{min}}{2}\right) \quad (5)$$

The gain offset a (in dB) is represented as

$$a = \delta_1(t - m\delta_2) \quad (6)$$

where δ_1 and δ_2 are normalised real uncertainties, and t and m characterise the top limit line of the exclusion region. For instance, the inner exclusion region in Figure 1 for the single loop analysis requires that t = 3 and m = 1.5. To cast this problem into a μ framework, it is necessary to convert these equations to the polar form $ae^{-j\phi}$, where the negative sign denotes phase lag. This gives

$$\begin{aligned} ae^{-j\phi} &= e^{c\delta_1(t-m\delta_2)-j(\gamma_1\delta_2+\gamma_2)} \\ &= e^{-j\gamma_2}e^{c\delta_1(t-m\delta_2)-j\gamma_1\delta_2} \end{aligned} \quad (7)$$

where c = (ln10)/20, $\gamma_1 = \frac{\phi_{max}-\phi_{min}}{2}$ and $\gamma_2 = \frac{\phi_{max}+\phi_{min}}{2}$
To generate the LFT-based uncertainty description, a first order Padé approximation is used:

$$e^{-Ts} = 1 - \frac{Ts}{1 + \frac{Ts}{2}} \quad (8)$$

where $-Ts$ is given by

$$-Ts = c\delta_1(t - m\delta_2) - j\gamma_1\delta_2 \quad (9)$$

This first order approximation is adequate for phase margins of up to 90°, and the resulting LFT model was seen to match the exclusion region used by the classical approach very closely, [11, 3].

For multi-loop analysis, the LFT-based uncertainty model described above is inserted in all loops simultaneously. In this case, however, the gain and phase margin requirements are 3 dB and 30° respectively and therefore, the parameters m and t from equation (6) are chosen as m = 1 and t = 2. The multi-loop criterion is then checked by scaling the exclusion region by applying a scaling factor to m, t, γ_1 and γ_2 until μ = 1. At this point, the gain and phase margins can be computed by back-substituting these values in equations (5) and (6).

Most published work on μ-analysis has assumed that μ is computed on a frequency sweep along the $s = j\omega$ axis. However, computing μ away from the imaginary axis can also provide a lot of useful information. In particular, the worst-case eigenvalue criterion can be checked by shifting the imaginary axis into the left and right half planes until an uncertainty combination is found which places a closed loop pole on the axis. Other tests are also possible, for example, by sweeping s_0 along a line of constant damping, such as $\xi = 0.4$, one may find the smallest perturbation which reduces damping below this level. Since k_m is typically discontinuous as s_0 moves from the real axis to neighbouring complex points, it is also useful to check stability along the real axis.

6 Analysis of the longitudinal HWEM dynamics

For the considered ranges of uncertainties, the worst-case eigenvalue criterion was satisfied for all seven flight conditions, and almost identical results were obtained using the μ-analysis and classical techniques. At a flight condition of 200 knots, for example, the nominal, μ worst-case and classical worst-case eigenvalue positions are shown in Table 2. Also shown in the table are the worst-case values of the uncertain parameters found using both approaches. Note that although the results are very similar, the μ worst-case uncertainty combination places all the eigenvalues slightly nearer the boundaries.

To compare the worst-case stability margin criterion results, Nichols curves were plotted for (i) the worst-case obtained using μ and (ii) every combination of the extreme points of the Five Category 1 uncertain parameters. It was found that for three flight conditions (110, 90 and 60 knots), the worst-case uncertainties did not lie on the extreme points of the parameters. Typical results are shown in Figure 6, which for clarity has been zoomed in Figure 7. It can be seen that the classical approach produces optimistic results, i.e. the worst-case Nichols plot found by μ is closer to the exclusion regions. Note also that the analysis at 110 knots using μ (Figures 6 and 7) generated a worst-case uncertainty of $\delta_{C_{m_q}}$ = 0.9845, $\delta_{C_{m_\alpha}}$ = 0.9976, $\delta_{C_{m_{tail}}}$ = 1, $\delta_{I_{yy}}$ = 0.0931 and $\delta_{X_{Dxcg}}$ = 0.1438. When the classical approach was used, the worst-case was found to be $\delta_{C_{m_q}}$ = 1, $\delta_{C_{m_\alpha}}$ = 1, $\delta_{C_{m_{tail}}}$ = 1, $\delta_{I_{yy}}$ = -1 and $\delta_{X_{cg}}$ = 1. The question then arises as to how important the last two uncertainties are, i.e, whether $\delta_{I_{yy}}$ and $\delta_{X_{cg}}$ have a significant effect on the stability margins. This question can be easily answered using the technique of μ-sensitivities, [12], which measures the relative importance of each uncertainty in the Δ set. In fact, evaluation of the μ-sensitivities for each uncertainty showed that $\delta_{X_{cg}}$ and $\delta_{I_{yy}}$ are actually the second and third most important elements in the set, [2, 3], implying that changes in the values of these two parameters will significantly affect the stability margins. Note again that the values of these parameters which give the true worst-case do *not* correspond to their maximum or minimum values. This phenomonon was repeated for all three of the flight conditions, and calls into question the implicit assumption made in the classical approach that the worst case will always correspond to some combination of the extrema of the uncertain parameters.

The computation times for finding the worst cases for (i) the classical approach using only minimum and maximum values of each parameter, and (ii) μ analysis with 100 frequency points, are plotted in Figure 8. As expected, the computation time for the classical approach increases exponentially with the number of uncertainties, so that for a Δ size > 8, μ is seen to be less computationally intensive than the classical technique. This fact becomes significant when we seek to also include Category 2 uncertainties in the analysis, or when we seek to analyse the effect of longitudinal and lateral uncertainties together.

Finally, we present sample results for the worst-case stability margin multi-loop analysis. At a flight condition of 90 knots,

the uncertainties associated with the elliptical Nichols exclusion regions were increased in each loop simultaneously until μ = 1. The corresponding gain and phase margins were found to be 13.97 dB and 37.86^o respectively. Using the classical approach, the corner points of the trapezoidal Nichols exclusion region were checked and the gain and phase margins were computed as 15.5 dB and 41.2^o respectively. It can be observed that the results obtained using the classical approach are more optimistic than those computed from μ, since every possible combination of the phase/gain offsets is considered in the μ-analysis, whereas the classical approach assumes the same phase/gain variations in each loop of the system. Furthermore, the μ-analysis imposes a slightly more stringent requirement on the computation of the phase and gain margins (since the elliptical exclusion regions used by μ are slightly bigger than the diamond-shaped exclusion regions used by the classical approach). A multi-loop μ-analysis was also carried out using the elliptical and trapezoidal Nichols exclusion regions at 150 knots. Both exclusion regions were scaled until the value of μ reached 1 and the resulting multivariable phase and gain margins were then computed. For the elliptical Nichols exclusion regions, a phase margin of 41.2^o and a gain margin of 4.18 dB were obtained. For the trapezoidal Nichols exclusion regions, a phase margin of 44.8^o and a gain margin of 4.5 dB were obtained. Again, it can be observed that the elliptical exclusion region is, as expected, slightly more conservative than the trapezoidal exclusion region.

7 Conclusions

This paper has described new μ-analysis tools for the clearance of flight control laws for highly augmented aircraft. Comparisons between the μ-analysis techniques and the classical industrial approach show that the new analysis tools can provide more rigorous (i.e. more accurate identification of worst-cases) and efficient (i.e. computationally faster) analysis of worst-case aircraft stability characteristics in the presence of multiple sources of parametric uncertainty.

References

[1] Korte, U., *Tasks and Needs of the Industrial Clearance Process*, Chapter 2 of *Advanced Techniques for Clearance of Flight Control Laws*, Fielding, C., et al, (Eds.), Springer Verlag, 2002.

[2] Bates, D.G, Kureemun, R. and Mannchen, T., "Improved Clearance of a Flight Control Law using μ-Analysis Techniques", *to appear in the Journal of Guidance, Control and Dynamics*, 2003.

[3] Kureemun, R., *μ-Analysis Tools for the Flight Clearance of Highly Augmented Aircraft*, Ph.D. Thesis, Department of Engineering, University of Leicester, November 2002.

[4] D'Mello, G., *The Harrier Wide Envelope Model*, GARTEUR Technical-Publication, TP-119-08, 2000.

[5] Ferreres, G., *A Practical Approach To Robustness Analysis*, Kluwer Academic/Plenum Publishers, 1999.

[6] Mannchen, T., Bates, D.G. and Postlethwaite, I., "Modelling and Computing Worst-Case Uncertainty Combinations for Flight Control Systems Analysis", *Journal of Guidance, Control and Dynamics*, Vol. 26, No. 6, pp. 1029-1039, 2002.

[7] Dijkgraaf, J.P. and Bennani, S., "Low Order LFT Modelling and Generation from the Non-Linear Equations of Motion of a Fighter Aircraft", *Proc. of the IEEE International Symposium on CACSD*, Glasgow, pp. 236-241, 2002.

[8] Deodhare, G. and Patel, V.V., 1998, "A 'Modern' Look at Gain and Phase Margins: an $\mathcal{H}^\infty$ / μ Approach", *Proc. of the AIAA Conference on GNC*, Boston, 1998.

[9] Kureemun, R., Bates, D. G. and Postlethwaite, I., "Quantifying the Robustness of Flight Control Systems using Nichols Exclusion Regions and the Structured Singular Value", *IMechE Journal of Systems and Control Engineering*, 215(16), 2001.

[10] Bates, D.G. and Postlethwaite, I., *Robust Multivariable Control of Aerospace Systems*, Delft University Press, 2002.

[11] Mannchen, T. and Well, K. H., *Uncertainty Bands Approach to LFT Modelling*, Chapter 13 of *Advanced Techniques for Clearance of Flight Control Systems*, Fielding, C., et al (Eds.), Springer Verlag, 2002.

[12] Braatz, R. D. and Morari, M., "μ-Sensitivities as an Aid for Robust Identification", *Proceedings of the American Control Conference*, Vol. 1, pp. 231-236, 1991.

Variable name	[Min,Max] value	Units
U_Xcg	[-1.72,-11.7]	%MAC
U_I_{yy}	[56887,69529]	kgm^2
U_$C_{m_{tail}}$	[-20,+20]	%
U_C_{m_q}	[-20,+20]	%
U_C_{m_α}	[-20,+20]	%

Table 1: Category I longitudinal uncertainties

classical w.c. eig.	μ w.c. eig.	classical w.c. uncertainties	μ w.c. uncertainties
-0.1985	-0.1980	1	0.9682
-0.1669	-0.1660	-1	-0.9985
-0.0631	-0.0630	1	0.9771
-8.5e-5+0.0775j	7.8e-5+0.0775j	-1	-0.9906
-8.5e-5-0.0775j	7.8e-5-0.0775j	1	0.9886

Table 2: Sample results for worst-case eigenvalue criterion at FC1

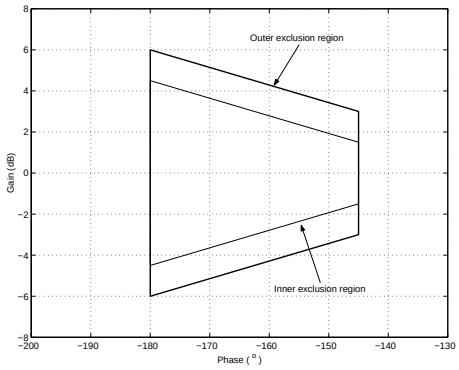

Figure 1: Nichols exclusion regions (single loop)

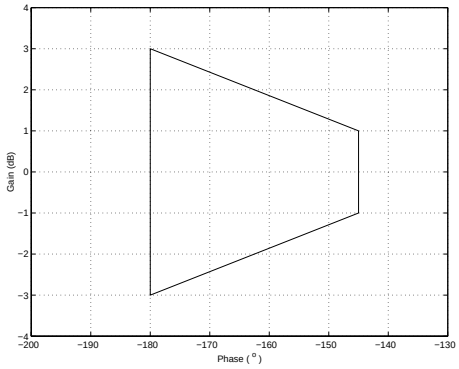

Figure 2: Nichols exclusion regions (multi-loop)

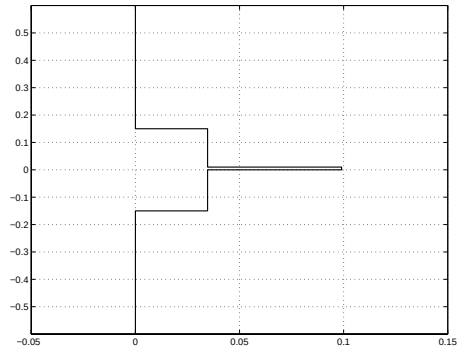

Figure 3: Boundaries for the unstable eigenvalue requirement

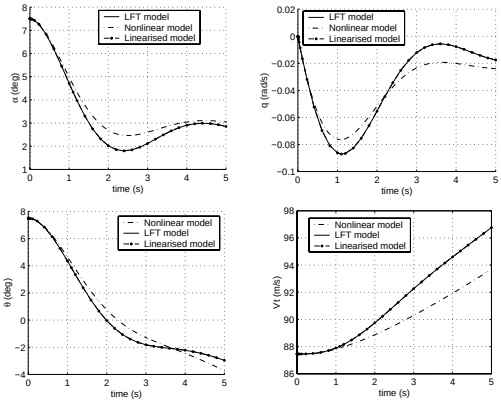

Figure 4: LFT validation (nominal case)

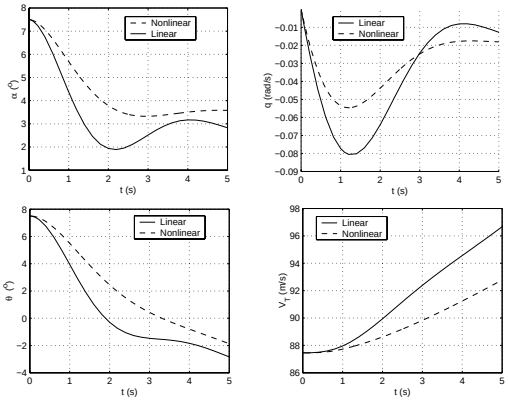

Figure 5: LFT validation for random values of the uncertainties

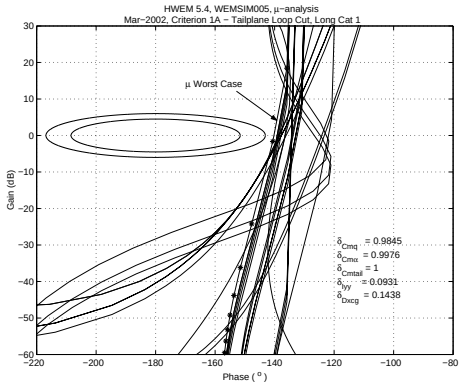

Figure 6: μ (-*-) and classical (-) worst cases

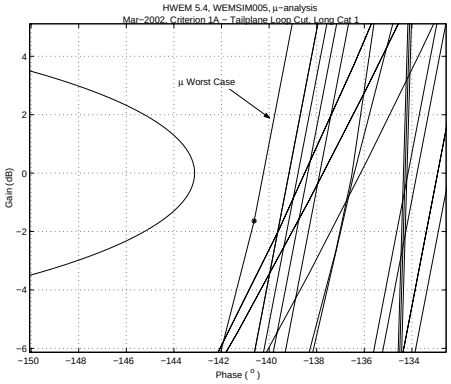

Figure 7: Close-up of Figure 6

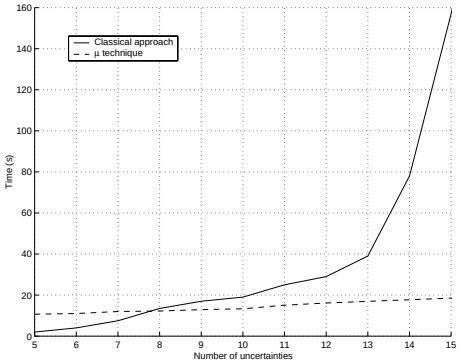

Figure 8: Computation times for μ and classical techniques